Analytica Chimica Acta 1139 (2020) 50–58

Contents lists available at ScienceDirect

Analytica Chimica Acta

journal homepage: www.elsevier.com/locate/aca

A non-enzymatic electrochemical biosensor for the detection of formalin levels in fishes: Realization of a novel comparator effect based on electrolyte

Priyannth Ramasami Sundhar Baabu [a, b], Parthasarathy Srinivasan [a, c], Arockia Jayalatha Kulandaisamy [a, c], Jeyashakila Robinson [d], Jeyasekaran Geevaretnam [e], John Bosco Balaguru Rayappan [a, c, *]

[a] Centre for Nanotechnology & Advanced Biomaterials (CeNTAB), SASTRA Deemed University, Thanjavur, 613 401, Tamil Nadu, India
[b] School of Chemical and Biotechnology (SCBT), SASTRA Deemed University, Thanjavur, 613 401, Tamil Nadu, India
[c] School of Electrical & Electronics Engineering, SASTRA Deemed University, Thanjavur, 613 401, Tamil Nadu, India
[d] Department of Fish Quality Assurance and Management, Tamil Nadu Dr. J. Jayalalithaa Fisheries University, Fisheries Colleges and Research Institute Campus, Thoothukudi, 628008, Tamil Nadu, India
[e] Tamil Nadu Dr. J. Jayalalithaa Fisheries University, Vettar-River View Campus, Nagapattinam, 611 002, Tamil Nadu, India

HIGHLIGHTS

- Electrochemical detection of formalin using CdS nanoparticles as nanointerface.
- Dynamic sensitivity based on electrolyte concentration showcasing a switch-like behaviour.
- A novel electrochemical comparator effect is reported.
- Heterogeneous rate constant and surface coverage are consistent with comparator effect.
- Threshold concentration of formalin to exhibit comparator effect is 14.845 mgL^{-1}.

GRAPHICAL ABSTRACT

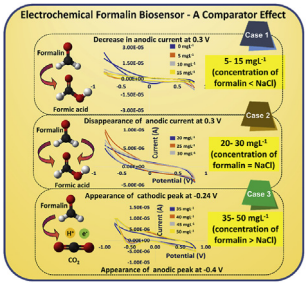

ARTICLE INFO

Article history:
Received 24 March 2020
Received in revised form
23 August 2020
Accepted 17 September 2020
Available online 20 September 2020

Keywords:
Formalin
Electrochemical biosensor
Comparator effect
CdS nanoparticles
Dynamic sensitivity

ABSTRACT

Formalin has been used as the preservative of fishes in the concentration range of 15–25 mgL^{-1}. However, there have been a high frequency of violations in the optimum use of formalin levels. The consumption of fishes treated with excessive formalin levels leads to nasopharynx, leukaemia and sinonasal cancer and there is a huge demand for the development of formalin sensor. Conventional formalin sensors such as chromogenic and mass balance sensors fall short in real-time analysis due to the lack of specificity and sensitivity in the interference medium. In this context, it has been emphasized to develop a non-enzymatic electrochemical biosensor with microwave synthesized CdS nanoparticles as a nanointerface owing to its surface limited kinetics. NaCl of 1 mM was considered as an electrolyte solution in the present study. Dynamic sensing characteristics with varying formalin levels of 5–50 mgL^{-1} was studied in three different concentration ranges as 5–15 mgL^{-1} (concentration of formalin < NaCl; conversion of formalin to formic acid), 20–30 mgL^{-1} (concentration of formalin ~ NaCl; equilibrium

* Corresponding author. , Centre for Nanotechnology & Advanced Biomaterials (CeNTAB), SASTRA Deemed University, Thanjavur, Ext: 2255, 613 401, Tamil Nadu, India.
E-mail address: rjbosco@ece.sastra.edu (J.B.B. Rayappan).

https://doi.org/10.1016/j.aca.2020.09.035

between the oxidative and reductive product), 35–50 mgL^{-1} (concentration of formalin > NaCl; complete oxidation of formic acid to CO_2). Hence, with the exhibition of such a dynamic sensitivity based on electrolyte, the developed biosensor acts as an electrochemical comparator showcasing a switch-like behaviour in detecting formalin levels. The threshold concentration of formalin required for the comparator effect was found to be 14.845 mgL^{-1}. The developed biosensor, most essentially, exhibited a versatility in quantifying formalin levels in real-time fish samples.

1. Introduction

Fishes are consumed globally as they contain large content of proteins and long chain n-3 polyunsaturated fatty acids [1]. However, sustaining the quality of fish is a major offspring and many preservatives have been adopted over the years for addressing this issue. One such preservative is formalin which stands effective in killing external parasites populating on the skin, fins and gills of the fish but displays poor efficiency against internal parasites as well as exogenous fungal and bacterial infections [2]. Formalin possesses the ability to deplete oxygen, where 5 mgL^{-1} of formalin can remove 1 mgL^{-1} of dissolved oxygen. In addition, storage of formalin at cold temperatures should be supervised with caution as formalin can transform into paraformaldehyde, an insoluble polyacetal form of formaldehyde that could potentially kill the fishes on contact.

Conventionally, fishes are given a formalin bath treatment, where dual pivotal rationale exists. If a prolonged bath is preferred, a low concentration of formalin (15–25 mgL^{-1}) is expected to be used or if a short bath is preferred (30–60 min), a high concentration (250 mgL^{-1}) of it is to be used [2]. Unfortunately, there have been high frequency of violations of the optimum use of formalin. Thus, consumption of fishes treated with excessive formalin levels leads to the adverse effects such as nasopharynx, leukaemia and sinonasal cancer owing to the carcinogenic behaviour of formalin [3]. Hence, it is imperative to design and develop a highly sensitive formalin sensor with desired figure of merits.

Over the years, several strategies have been deployed towards sensing formalin levels. Chromogenic sensors using functionalized thiol and bulky polar polyamines exhibited a limit of detection (LOD) of 36 ppb in water [4]. Mass balance sensors incorporating quartz crystal microbalance coated with polyvinyl amine modified electro spun polyacrylonitrile nanofibers displayed a LOD of 500 ppb. These sensors showed a promising results towards development of point-of-care devices for formalin sensing [5]. However, these sensors are not reliable for real-time monitoring of formalin levels in fishes. Chromogenic sensors fall short owing to the selection of chromophores, media and indicator [6]. Similarly, mass balance sensors are not quite affordable in practical scenario because of their lack of sensitivity and specificity in the interference environment [7].

In this background, electrochemical formalin sensors are gaining attention owing to the availability of an array of parameters that could be measured for analysis and subsequent quantification of the levels, precisely. The conversion of formalin to formate is a specific and integral step in the methane metabolism found in prokaryotes predominantly catalysed by formaldehyde dehydrogenase (FDH), an oxidoreductase enzyme [8].

Various enzymatic electrochemical biosensors incorporating FDH have been reported, such as gold nanoparticles and chitosan modified glassy carbon electrode (GCE) with methylene blue as indicator [9], NAD^+ and Nafion modified gold electrode [10], mesoporous silica and quinone modified glassy carbon electrode (GCE) and poly (glycidyl methacrylate-*co*-3-methylthienyl methacrylate) and polypyrrole modified GCE [11]. Also, a conductometric biosensor incorporating alcohol oxidase instead of FDH has been reported [12].

In addition, few non-enzymatic electrochemical formalin sensors are reported. Amperometric chemiresistive sensor incorporating single walled carbon nanotubes (CNTs) and hydroxylamine [13], impedimetric sensor fabricated with biomimetic electrospun nanofibers decorated with CNTs [14], gold cluster modified screen printed electrodes [15] and electrodeposited Pt–Pd alloy as nanostructures on a Nafion modified GCE [16]. Hence, this stood as the first step of our motivation to develop a non-enzymatic electrochemical biosensor employing cadmium sulphide (CdS) nanoparticles as a nanointerface owing to its idiosyncratic catalytic properties for enhancement of the electron transfer in an otherwise diffusion limited kinetics, usually significant in terms of electrochemical biosensing [17]. Also, being a direct bandgap semiconducting material with a band gap of ~2.42 eV, the number of electrons transferred from the valence band to the conduction band when present in the form of nanoparticles is controlled, proves essential for elevated faradaic response during sensing [18]. Chitosan was chosen as the binder owing to its ability to get protonated in the presence of acetic acid and hence stabilize the nanocomposite interface binding through electrostatic interactions.

Hence, in the present study, we have synthesized CdS nanoparticles using microwave technique and characterized for their morphology and structure. Furthermore, Cyclic Voltammetry (CV) was the sole technique used to characterize the electrochemical properties of the modified working electrode towards detection of formalin. The fabricated electrode ended up furnishing a novel sensing mechanism for formalin along with a comparator effect due to variations in the background limit (concentration of NaCl), which was vindicated using CV studies at optimized scan rates.

2. Materials and methods

2.1. Chemicals used

Cadmium acetate (Cd $(CH_3COO)_2$), 99.5%, Loba Chemie), thiourea (CH_4N_2S, 99.5%, Fischer Scientific), chitosan, acetic acid (reagent plus ≥ 99%, sigma Aldrich), sodium chloride (Bioxtra ≥99.5%, Sigma Aldrich) and formaldehyde (37–41% w/v, Merck) were used. All the reagents and solutions were prepared using deionized water (Millipore, USA).

2.2. Synthesis of CdS nanoparticles

The synthesis of CdS nanoparticles was carried out by microwave assisted preparation in an aqueous medium. To begin with, cadmium acetate and thiourea were taken in the ratio 2:1 owing to the weak dissociation ability of acetate precursors in water. The precursors were dissolved in 250 mL deionized water and subsequently kept at constant stirring at 350 rpm for 10 min. The

prepared aqueous solution was kept in the microwave oven for 1 h at a microwave power of 450 W. During microwave irradiation, colour of the solution was changed to bright yellow vindicating the formation of CdS nanoparticles. The obtained nanoparticles were then annealed at 80 °C for 24 h.

2.3. Characterization of CdS nanoparticles

X-Ray Diffractometer (XRD) (Model: D8 Focus, Bruker, Germany) was used to investigate the structural properties of the synthesized CdS nanoparticles. Cu $K\alpha_1$ with a wavelength of $\lambda = 1.5406$ Å was used as the source of X-Rays in the 2θ range of 20–80°. Morphological studies of the nanoparticles were performed using Field Emission Scanning Electron Microscope (FE-SEM) (Model: JEOL, 6701F, Japan) and Field Emission Transmission Electron Microscope (FE-TEM) (Model: JSM2100, JEOL, Japan). The samples used for SEM and TEM analysis were prepared by dispersion of the nanoparticles in ethanol followed by subsequent coating on a carbon coated copper grid. Elemental analysis was carried-out using the Energy Dispersive X-Ray Spectroscopy (EDS) integrated along with the FE-SEM system. Functional group analysis of the nanoparticles was performed using Fourier Transform Infrared Spectrometer (FT-IR) (Model: Bruker, Alpha-T, Germany) in the range of 400 and 4000 cm^{-1}. The binding energies and atomic surface concentrations of Cd and S were obtained using X-Ray Photoelectron Spectroscopy (XPS) analysis (Model: K-alpha, Thermo Scientific, USA). The specific surface area of the CdS nanoparticles were determined using Nitrogen adsorption-desorption isothermal analysis, which was performed at −196 °C with the Autosorb-1, Quantachromeanalyzer. The specific surface area of the sample was then calculated using the BET method.

2.4. Electrochemical analysis

The electrochemical measurements were carried out using CHI700D Electrochemical Analyzer (CH Instruments, USA) employing a three electrode system consisting of a platinum wire as the auxiliary electrode (CHI115, CH Instruments, USA), an Ag/AgCl electrode (CHI111, CH Instruments, USA) saturated with 1 M KCl as reference electrode and platinum electrode as working electrode (2 mm diameter, CHI104, CH Instruments, USA). The choice of Pt electrode as the working electrode for this study is based on the fact that the work function of platinum ($\varphi_0 = 6.35$ eV) is high compared to the gold electrodes.

2.4.1. Fabrication of Pt/CdS/Chitosan electrode

CdS nanoparticles were dispersed in 100 μL of deionized water. 100 μL of 0.5% w/v chitosan in 0.2% v/v acetic acid along with the CdS dispersed solution were sonicated for 2 h to yield homogeneous dispersion of the nanoparticles. From this solution, 3 μL was taken, drop casted over the platinum electrode and allowed to dry at room temperature for 2 h. Cyclic Voltammetry studies were carried out in a 20 mL electrochemical cell with electrolyte solution of 1 mM of 5 mL NaCl. All CV studies were performed at room temperature in the potential window of −0.8 V to +0.8 V.

Dynamic sensing characteristics with varying formalin levels of 5–50 mgL^{-1} was studied in three different concentration ranges as 5–15 mgL^{-1}, 20–30 $mgL^{-1}$and, 35–50 mgL^{-1}.

2.4.2. Real-time analysis with Indian Mackeral fishes

Indian Mackeral fishes (2 Nos) were purchased from the local fish market at Thanjavur, India. These fishes were kept in ice and transported to the laboratory within 30 min and then rinsed with tap water. A fish sample with a size of 20 mm × 20 mm was cut down using forceps and homogenized thoroughly to yield a turbid solution. Formalin levels of 5–20 mgL^{-1} were spiked to this solution for carrying out the electrochemical analysis using Cyclic Voltammetry in the 20 mL electrochemical cell with electrolyte solution of 1 mM of 5 mL NaCl at 100 mV/s scan rate.

3. Results and discussion

3.1. Characterization of CdS nanoparticles

XRD pattern of the prepared CdS nanoparticles is shown in Fig. 1 (a). It revealed the formation of polycrystalline natured face centred cubic crystal structure of CdS with lattice parameters of a = b = c = 5.832 Å. The observed pattern is in good agreement with the JCPDS card data (65–2887). The preferential plane of orientation was found to be along (1 1 1) plane. Crystallite size (D) of the CdS nanoparticles was calculated using Debye-Scherrer's formula from Eq. (1).

$$D = \frac{180}{\pi} * \frac{k * \lambda}{FWHM * \cos\theta} \quad (1)$$

where, k refers to the shape factor (k = 0.9), λ refers to the wavelength of the used X-rays (1.5406 Å), FWHM refers to the full width at half maximum and θ is the Bragg's angle. The average crystallite size of the synthesized CdS nanoparticles was found to be 6 nm, laying the required grounds for enhanced electron transfer between CdS and the working electrode. The other structural properties such as lattice contraction (ε) and texture coefficient ($T_{c(hkl)}$) were calculated and discussed in supporting information (ES1).

Surface morphology of the CdS nanoparticles is shown in Fig. 1 (b). The synthesized CdS nanoparticles exhibited an aggregated spherical morphology with average grain size distribution of 56 nm (Fig. 1 (b) Inset figure). It is known that microwave radiation facilitates nucleation and growth of nanoparticles by predominantly two mechanisms, namely, dipolar polarization and ionic conduction [19]. Thus, in a reaction system consisting of heterogeneous reactants, in this case, cadmium acetate and thiourea, selective heating of the precursors resulted in inhomogeneous energy dispersion and temperature gradients. As a result, heat transfer from regions of high temperature called hotspots to lower temperature regions resulted in a heat conduction [19]. Hence, the heat conduction rate that decides the growth of the nanoparticles. Consequently, the plausible reason for the observed aggregation of the nanoparticles could be attributed to the presence of higher gradients. The possible reaction for the formation of CdS nanoparticles is given in Eq. (2) as,

$$NH_2CSNH_2 + H_2O \rightarrow NH_2CONH_2 + H_2S$$

$$H_2S \rightarrow 2H^+ + S^{2-}$$

$$Cd^{2+}(from\ Cd\ acetate) + S^{2-} \rightarrow CdS \quad (2)$$

Elemental analysis from the EDAX mapping confirmed the presence of cadmium and sulphur elements with corresponding wt % of 10.25 and ~3.57% respectively (ES2). FTIR spectra of the CdS nanoparticles is shown in Fig. 1 (c). The peak at 600 cm^{-1} is due to Cd–S stretching mode [18]. The peak at 786 cm^{-1} is attributed to C–H bending, which is seen as a sharp peak in the spectra [20]. The feeble peaks at 1449 and 1648 cm^{-1} is assigned to C–N asymmetric stretching and amine N–H bending respectively. The peak at 3326 cm^{-1} is accredited to N–H stretching [20].

TEM images of CdS nanoparticles are shown in Fig. 2. The micrograph confirmed the formation of clustered spherical nanoparticles, whose average grain size distribution is in good

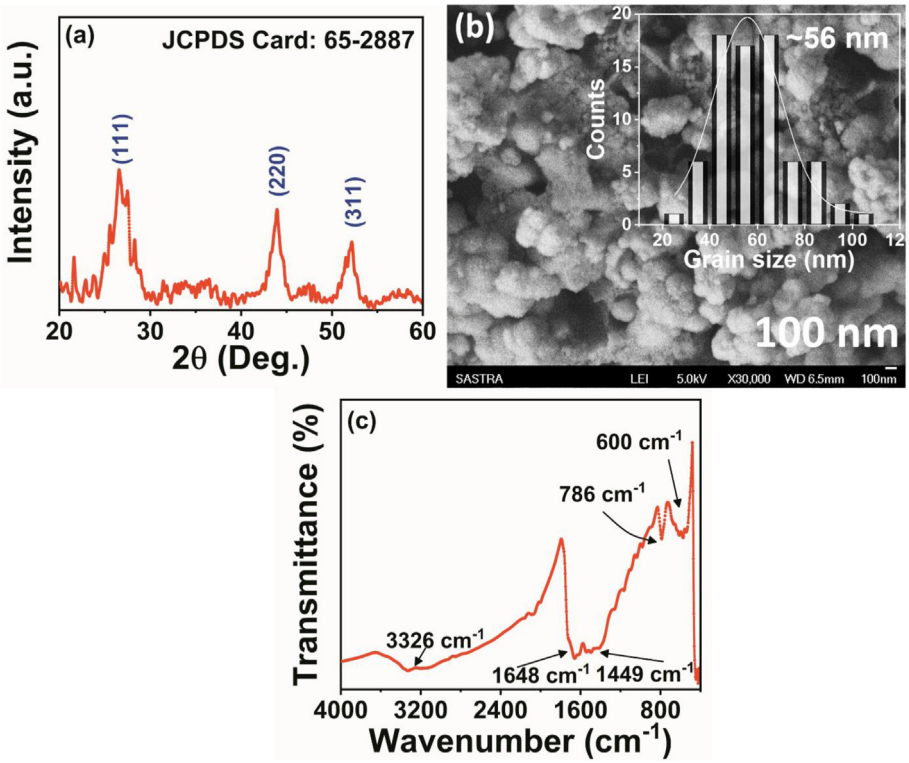

Fig. 1. (a) XRD pattern of CdS nanoparticles representing polycrystalline natured cubic crystal phase, (b) SEM image visualizes the formation of CdS nanoparticles of spherical shape (Inset figure: grain size distribution histogram exhibiting the size distribution of 56 nm), and (c) FTIR spectra of CdS nanoparticles representing the corresponding functional groups.

agreement with the SEM analysis (Fig. 1 (b) Inset figure). Fig. 2 (b) shows the SAED pattern which further confirmed the polycrystalline behaviour of CdS nanoparticles. Interatomic distance was observed to be 4.92 Å from the lattice fringes and it is in good agreement with the d-spacing obtained from XRD for (1 1 1) plane.

Nitrogen adsorption-desorption isothermal analysis of CdS nanoparticles is shown in Fig. 3 (a), which exhibited a type II adsorption isotherm. This indicates that at low temperature and high pressure, the lower thermal energy of nitrogen gas molecules resulted in increased availability of these molecules near to the surface and subsequent establishment of a multilayer adsorption [21]. From the BET analysis, C value was found to be much greater than 1 (~61) defining the obtained isotherm to be type II, which has a characteristic intermediate flat region attributed to a monolayer formation. BET surface area was found to be 5.25 m^2/g, indicating a high surface area material pivotal for enhanced electron transfer properties.

The XPS spectra of CdS nanoparticles is shown in Fig. 3(b–d). Survey spectrum confirmed the presence of Cd and S from the peaks observed at 405.16 and 162.03 eV respectively. The calculated peak areas of Cd and S revealed the atomic percentage of Cd and S as 47.10% and 52.90% respectively. Cd 3d spectrum shown in Fig. 3 (c) comprised of spin orbit doublet at 411.95 and 405.16 eV corresponding to Cd $3d_{3/2}$ and $3d_{5/2}$ respectively. The binding energy difference between Cd $3d_{3/2}$ and Cd $3d_{5/2}$ was found to be 6.789 eV, which confirmed the +2-oxidation state of Cd. On the other hand, sulphur exhibited spin orbit doublet at 162.03 and 163.08 eV corresponding to S $2p_{3/2}$ and S $2p_{1/2}$ respectively (Fig. 3 (d)).

3.2. Electrochemical bio-sensing of formalin

3.2.1. Multilayer confirmation

To confirm proper and uniform coating of the nanoparticles and matrix onto the Pt electrode, CV studies were carried-out and shown in Fig. 4 (a). As expected, the successive layers of matrix and nanoparticles were coated uniformly in 1 mM NaCl electrolyte. It could be seen that for 0.01 V/s scan rate, the reduction peak for bare Pt occurred at −0.295 V while that of CdS modified Pt (Pt/CdS) occurred at −0.316 V with a reduction in the current indicating the influence of CdS nanoparticles as barrier for hydrogen ions and oxygen to reach the electrode in the latter case [22]. A similar effect was observed for the oxidation peak as well, which occurred at −0.608 V for bare Pt and −0.623 V for CdS modified electrode. However, the redox peaks observed in the above two cases disappeared for the Pt/Chitosan/CdS coated electrode indicating the barrier effect induced as a result of chitosan. The redox peaks observed in the bare Pt case could be attributed to the reduction of hydrogen ions to hydrogen and water oxidation to hydroxyl ions respectively [23].

3.2.2. Optimization of scan rate

The scan rate optimization studies were employed using CV, as shown in Fig. 4 (b & c). For the bare Pt electrode in 1 mM NaCl electrolyte, at scan rates between 10 and 100 mV/s, the current increased linearly with the square root of scan rate for both the reduction and oxidation reactions, indicating a diffusion-controlled kinetics. (Fig. 4 (b)). However, in the case of Pt/Chitosan/CdS modified electrode in 1 mM NaCl electrolyte, the reduction current disappeared and the oxidation peak was obtained at near zero positive values, possibly due to hydrogen oxidation, evident from Fig. 4 (c). Here, the current increased linearly with the scan rate, indicating a surface-controlled kinetics, plausibly due to the introduction of CdS nanoparticles resulting in an enhanced electron transfer to the electrode.

When formalin (5 mgL^{-1}) was added to the reaction system, the current had a linear relationship with the scan rate giving rise to a

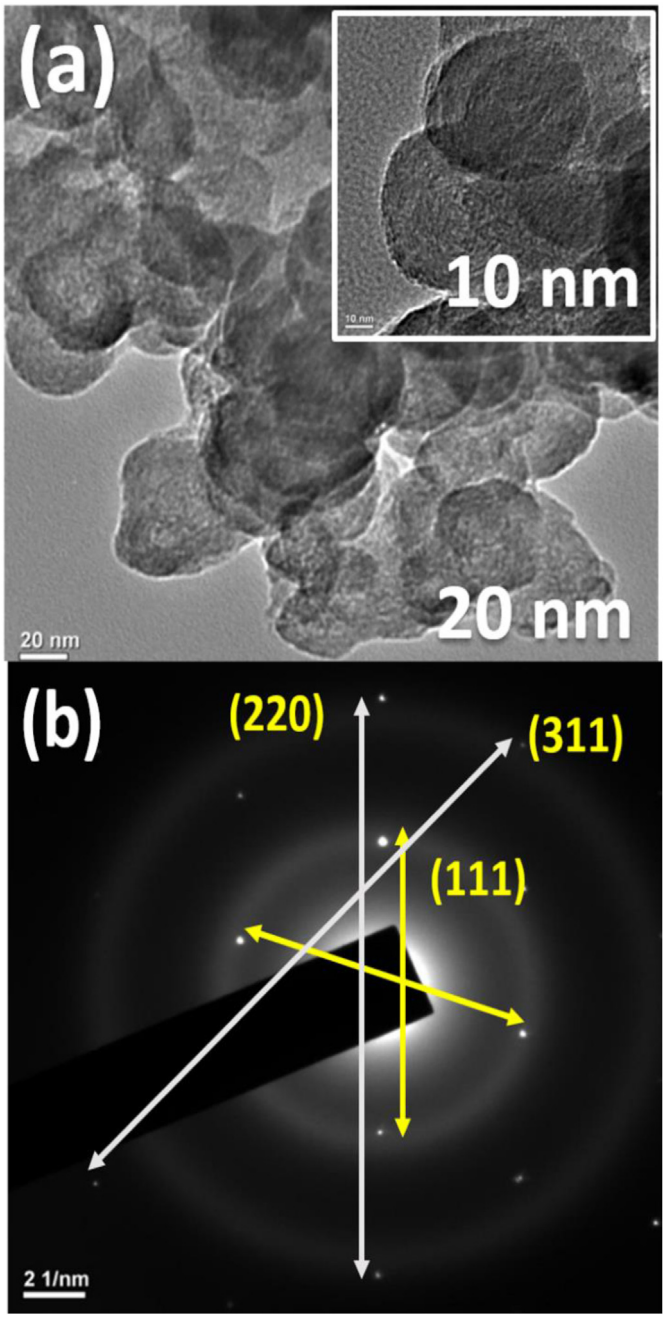

Fig. 2. (a) TEM image of CdS nanoparticles (inset image depicts the formation of spherical nanoparticles), and (b) SAED pattern of CdS nanoparticles represents the polycrystalline behaviour from the planes (1 1 1), (2 2 0) and (3 1 1).

surface-controlled kinetics in the case of Pt/Chitosan/CdS modified electrode, observed from Fig. 5 (a). However, as the concentration of formalin was increased to 50 mgL^{-1} in the same reaction system (Fig. 5 (b)), there was a gradual transition to a diffusion-controlled kinetics with an appearance of a cathodic peak near −0.2 V, like the bare Pt case. This could be possibly attributed to dynamic changes in the background limit with the concentration of formic acid increasing with increase in formalin concentration, thereby replenishing the reaction system with more hydrogen ions.

3.2.3. Electrochemical detection of formalin by Pt/Chitosan/CdS electrode - Comparator effect

The Pt/Chitosan/CdS modified electrode was then examined to detect the presence of formalin (100 μL) in 1 mM NaCl electrolyte. From Fig. 6 (a, b and c), interesting anodic profiles was observed similar to a comparator effect. For concentrations of formalin in the range between 5 and 15 mgL^{-1}, the anodic peak was observed at 0.3 V while for formalin in the range 20–30 mgL^{-1}, the peak disappeared. On the other hand, for the formalin in the range 35–50 mgL^{-1}, anodic peak at −0.4 V was observed. This could be attributed to the interplay of competition effect wherein in the first concentration range, the formalin levels are much lesser (5 mgL^{-1} – 0.166 mM, 10 mgL^{-1} – 0.332 mM and 15 mgL^{-1} – 0.499 mM) than the electrolyte concentration (1 mM). As a result, with increasing concentration in this range, the current decreased due to the increased formation of formic acid (oxidative product), thereby exhausting and suppressing the available hydrogen ions (reductive product from water), whose effect is minimal in 5 mgL^{-1} and maximal in 15 mgL^{-1}. Eq. (3) corresponds to the redox reaction in the above case,

$$HCHO + H_2O \rightarrow HCOOH + 2H^+ \quad (3)$$

Considering the second concentration range 20–30 mgL^{-1} (20 mgL^{-1} – 0.665 mM, 25 mgL^{-1} – 0.832 mM, 30 mgL^{-1} – 0.998 mM), no significant redox changes was observed because the oxidative product and the reductive product were equally present in concentration thereby establishing an equilibrium. But for concentrations more than 35 mgL^{-1} (>1 mM), the effect of weak formic acid upholds with complete disappearance of the peak at 0.3 V. Rather, a peak at −0.4 V was observed, which corresponds to the oxidation of formic acid as shown in the Eq. (4),

$$HCOOH \rightarrow CO_2 + 2H^+ + 2e^- \quad (4)$$

Hence, with the exhibition of such a dynamic sensitivity towards the electrolyte concentration, the developed Pt/Chitosan/CdS modified biosensor acts as an *electrochemical comparator* showcasing a switch-like behaviour while detecting levels of formalin. We have repeated the cyclic voltammetry studies in triplicate (Fig. ES3) and observed the comparator effect in all the three cases, validating the reproducibility of the observed mechanism and no interference of chitosan in the presence of formalin.

3.2.4. Electrochemical analysis of the comparator effect

The results of the detailed electrochemical analysis of the comparator effect are highlighted and presented in Tables 1 and 2. In the case of bare Pt and 1 mM NaCl, with respect to the cathodic reaction, the formal potential E° and over potential η increased with the concentration of formalin.

As these parameters evaluate the energy supplied for thermodynamically feasible redox reaction, such a trend was observed indicating a lower availability of hydrogen ions due to weak dissociative nature of formalin.

The charge Q_c, referring to the charge involved in the faradaic processes, was found to be decreased again indicating the lower availability of hydrogen ions. This observation along with increased Full Width at Half Maximum (FWHM), correspond to a transition from quasi-reversible to irreversible nature of the reaction indicating a chemical reaction initiated by an electron transfer involving association or dissociation. The heterogenous rate constant, K_s was also found to be increased with increasing concentration of formalin, which is associated with acceleration of the reaction complemented with increasing η. Surface coverage, Γ was observed to be decreased with increasing concentrations of formalin, vindicating the above-mentioned rationale for E°, η and Q_c. The Gibbs' free energy (ΔG) for this reaction was calculated to be −5.467 kJ/mol, indicating it to be a spontaneous reaction requiring an enhancement in the electron transfer.

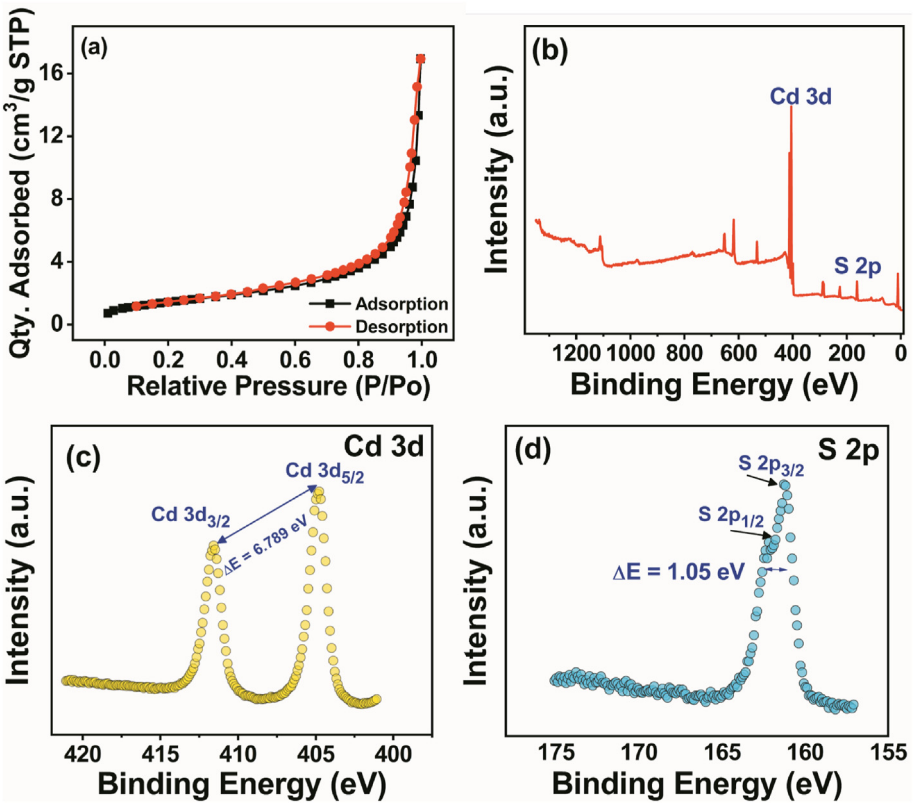

Fig. 3. (a) Nitrogen adsorption-desorption isotherm for CdS nanoparticles, XPS spectra of CdS nanoparticles (b) survey scan indicates the presence of both Cd and S elements in respective percentages of 47.10 and 52.90%, (c) Cd 3d spectra exhibiting spin orbit doublet of Cd3d$_{3/2}$ and Cd 3d$_{5/2}$ and, (d) S 2p spectra consists of S 2p$_{3/2}$ and S 2p$_{1/2}$ respectively.

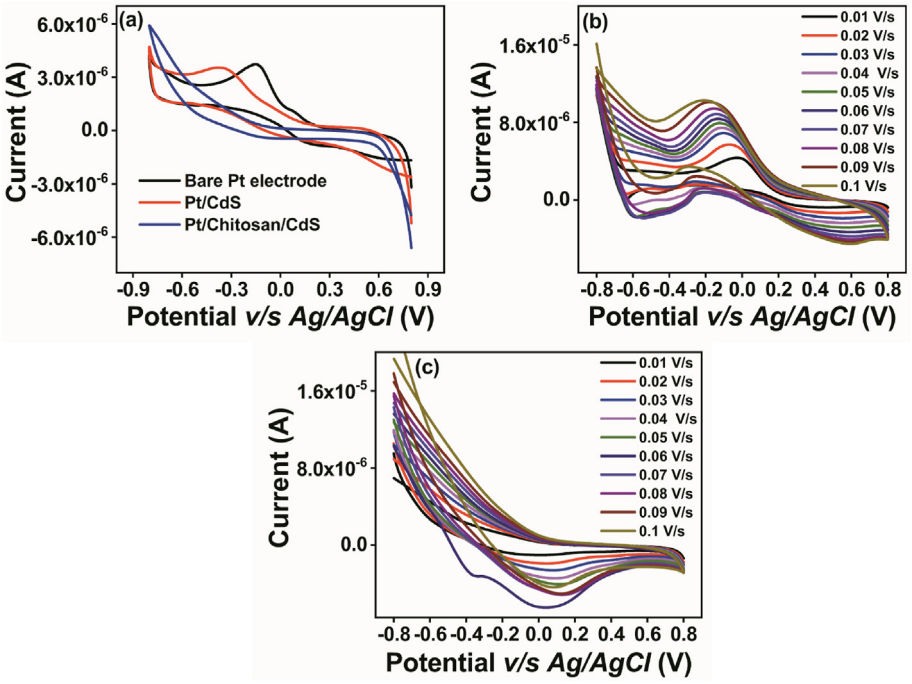

Fig. 4. (a) CV graph of bare Pt electrode, Pt/CdS, and Pt/Chitosan/CdS in 1 mM NaCl electrolyte at a scan rate of 0.01 V/s, exhibiting redox peaks at −0.295 & −0.608 V and −0.316 &-0.623 V for bare Pt and Pt/CdS respectively, and CV graphs at different scan rates between 10 and 100 mV/s of (b & c) bare Pt electrode and, Pt/Chitosan/CdS modified electrode in 1 mM NaCl electrolyte representing a diffusion-controlled kinetics and a surface-controlled kinetics respectively.

In the case of anodic reaction characterized by oxidation of water to hydroxyl ions, E° and η decreased with increasing formalin concentration indicating the increased availability of hydroxyl ions, in contrast to the cathodic case. Q_c and FWHM were found to

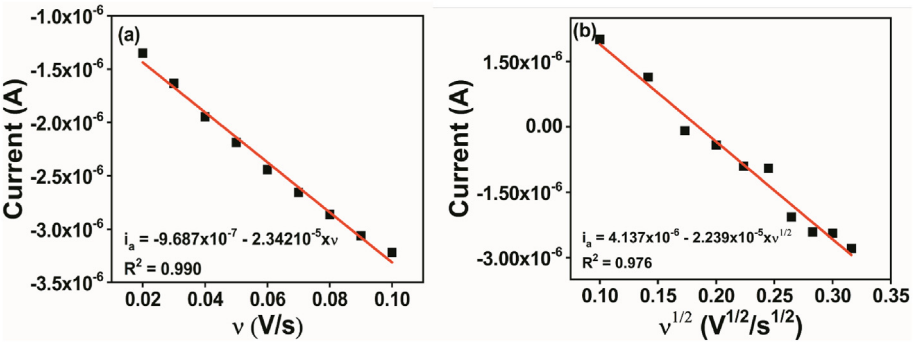

Fig. 5. Scan rate relationship of Pt/Chitosan/CdS modified electrode in NaCl in the presence of (a) 5 mgL^{-1}, and (b) 50 mgL^{-1} of formalin representing a transition of surface-controlled kinetics to a diffusion-controlled kinetics from 5 to 50 mgL^{-1}.

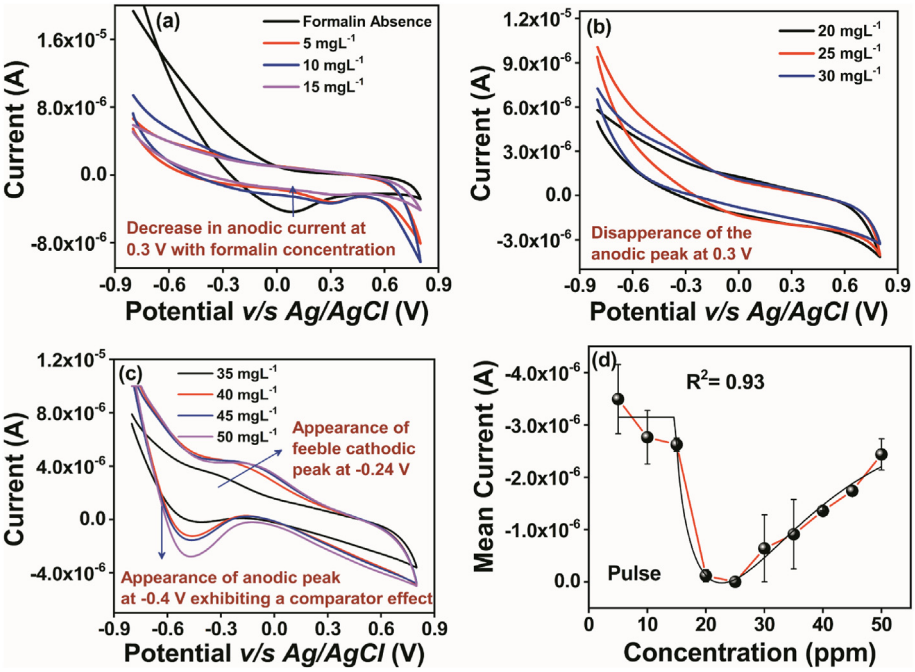

Fig. 6. CV graphs of Pt/Chitosan/CdS modified electrode in 1 mM NaCl in the presence of (a) 5–15 mgL^{-1}, (b) 20–30 mgL^{-1}, and (c) 35–50 mgL^{-1} of formalin exhibiting an electrochemical comparator effect, and (d) calibration curve of Pt/Chitosan/CdS biosensor towards the concentration range of 5–50 mgL^{-1} of formalin.

Table 1
Calculated electrochemical parameters for bare Pt electrode in 1 mM NaCl electrolyte.

Formalin Concentration	Absence of formalin		5 mgL^{-1} (0.166 mM)		20 mgL^{-1} (0.665 mM)		50 mgL^{-1} (1.664 mM)	
	Cathodic	Anodic	Cathodic	Anodic	Cathodic	Anodic	Cathodic	Anodic
E_c (V)	−0.198	0.594	−0.171	−0.388	−0.186	−0.362	−0.214	−0.408
E^0 (V)	−0.031	0.498	0.040	0.101	0.050	0.059	0.050	0.070
η (V)	−0.166	0.096	−0.211	−0.489	−0.235	−0.421	−0.264	−0.477
Q_c (μC)	−20.170	−26.741	−19.640	0.763	−15.530	−0.212	−13.080	−1.095
FWHM (V)	0.288	0.293	0.326	0.355	0.480	0.293	0.461	0.245
K_s (s^{-1})	0.324	0.743	0.363	0.013	0.282	1.109	0.484	1.105
S.C (μmol/cm^2)	2.172E-08	3.348E-08	1.567E-08	3.594E-11	1.549E-08	1.325E-11	7.856E-09	2.945E-10

decreased with formalin concentration, indicating a transition from irreversible to quasi-reversible nature of the reaction as a result of increased availability of the hydroxyl ions. K_s was also decreased substantiating the above transition in the nature of the reaction. However, Γ was decreased, possibly due to the occupation and eventual saturation of limited number of sites on the bare electrode to facilitate the electron transfer. ΔG was found to be 3.200 kJ/mol, indicating the reaction to be non-spontaneous and supporting the above-mentioned transition to quasi-reversible nature. With regards to Pt/Chitosan/CdS modified biosensor, the anodic reaction was characterized by the oxidation of formic acid. Here, E° increased from formalin absence to 5 mgL^{-1}, decreased to 0 at 20 mgL^{-1} and then increased till 50 mgL^{-1} with a shift from 32 mV to −572 mV. η exhibited a similar trend as E° without any

Table 2
Calculated electrochemical parameters for Pt/Chitosan/CdS modified electrode in 1 mM NaCl electrolyte.

Formalin Concentration	Absence of formalin		5 mgL^{-1} (0.166 mM)		20 mgL^{-1} (0.665 mM)		50 mgL^{-1} (1.664 mM)	
	Cathodic	Anodic	Cathodic	Anodic	Cathodic	Anodic	Cathodic	Anodic
E_c (V)	–	0.079	–	0.319	–	–	−0.240	−0.467
E^0 (V)	–	0.032	–	0.167	–	–	−0.201	−0.572
η (V)	–	0.047	–	0.151	–	–	−0.040	0.104
Q_c (μC)	–	−3.442	–	−10.256	–	–	−10.428	13.044
FWHM (V)	–	0.259	–	0.158	–	–	0.235	0.256
K_s (s^{-1})	–	0.219	–	0.582	–	–	0.269	0.396
S.C (μmol/cm^2)	–	5.557E-09	–	7.303E-09	–	–	5.086E-08	2.446E-08

characteristic shift. Q_c and FWHM were also increased, corresponding to a dual transition from quasi-reversible to irreversible to quasi-reversible nature, These observations justify the comparator effect. K_s followed the trend of E° where the rate of reaction was enhanced with formalin addition initially and it get hindered due to comparator effect. Γ was increased, justifying the role of CdS nanoparticles in creation of large number of active sites for enhanced electron transfer. ΔG was found to be −2.984 kJ/mol, indicating the reaction to be spontaneous and requiring much lesser free energy than the bare Pt case, essential for a biosensor.

3.2.5. Calibration-curve

Fig. 6 (d) shows the calibration curve of the developed Pt/Chitosan/CdS modified biosensor towards formalin detection. From the curve it is inferred that, the current decreased and saturated below the formalin threshold concentration of 14.84 mgL^{-1}. However, the current increased with increasing concentrations of formalin beyond this threshold level indicating a switch-like behaviour of the system [24,25]. Table 3 compares the figure of merits of the present work with the available literatures in which the present work stands novel in exhibiting a novel comparator effect with a minimum detection limit of 5 mg L^{-1}.

Aini et al. [9], Herschkovitz et al. [24] and Ozoner et al. [25] developed enzymatic electrochemical biosensors for detection of formalin. The major shortcoming of these works lies in the utilization of many components for biosensing, especially the enzyme formaldehyde dehydrogenase immobilized over polymer components. Notwithstanding their high specificity and lower detection limit than our biosensor, the stability of such enzymes and organic components in the presence of native salt environments is low. As a result, such systems cannot be extrapolated to real-time sensing of formalin.

On the other hand, considering the non-enzymatic electrochemical sensors developed by Dai et al. [14], Baez-Gaxiola et al. [15] and Zhou et al. [16] which reported wide linear ranges of detection and sensitivity, their applicability in real-time analysis like fish quality analysis is shallow. Our sensor possesses a linear range of detection within the range of 5–50 mgL^{-1} during the real-time analysis. Furthermore, the novelty of this study stands in the mechanism of detection of formalin, which provides two levels of detection schemes to the user. The first level being the qualitative confirmation of presence of formalin in the given sample using the novel comparator effect, followed by the second level of quantitative reporting of the level of formalin present in the given sample. Such a detection scheme is intuitive and realistic from a user's perspective.

3.2.6. Real-time sample analysis

Fig. 7 shows the CV trends corresponding to spiking of different formalin levels of 5–20 mgL^{-1} in the fish sample solution along with un-spiked sample as a control. From the curve, it is inferred that, the un-spiked fish sample exhibits a similar CV trend to those obtained for the first concentration range (5–15 mgL^{-1}), as presented in section 3.2.3. This revealed the presence of formalin levels even in the un-spiked fish sample. Also, from this result it is conceivable to quantify the presence of formalin levels in the un-spiked fish sample between the concentration range of 5–15 mgL^{-1}. Upon spiking formalin levels from 5 to 20 mgL^{-1} to the fish sample, a potential shift to −0.4 V along with an increase in current with formalin concentrations was observed. Such an observation stands similar to that observed for the third concentration range (>35 mgL^{-1}) as in the case of testing the modified electrode towards various concentrations of formalin. Thus, the developed electrochemical biosensor exhibits a versatility in quantifying the real-time formalin levels with the observed comparator effect. We strongly believe that our work stands as a preliminary study towards development of such intuitive real time sensors for formalin detection in fishes.

Table 3
Comparison of the present work with available literature.

Base electrode + biosensor components	Detection method	Electrochemical method adapted	Linear Range	Detection limit	Ref.
Glassy carbon electrode + ionic liquid + gold nanoparticles + chitosan	Enzymatic	Differential Pulse Voltammetry (DPV)	0.01–10 mg L^{-1}	0.1 mg L^{-1}	[8]
Glassy carbon electrode + poly (methacryloylhydrazide) electrospun nanofibers + CNTs	Non-enzymatic	Electrochemical Impedance Spectroscopy (EIS)	30 μ gL^{-1} – 300 mg L^{-1}	24 μgL^{-1}	[13]
Carbon screen printed electrodes + catalytic gold clusters	Non-enzymatic	Cyclic Voltammetry (CV)	30 μ gL^{-1}- 300 mg L^{-1}	27 mg L^{-1}	[14]
Glassy carbon electrode + Nafion + bimetallic Pt–Pd nanoparticles	Non-enzymatic	Cyclic Voltammetry (CV)	300 μ gL^{-1}– 30 mg L^{-1}	90 μ gL^{-1}	[15]
Carbon screen printed electrodes + $Os(bpy)_2$-poly (vinylpyridine) + formaldehyde dehydrogenase	Enzymatic	Amperometry	30 μ gL^{-1}– 1.5 mg L^{-1}	30 μ gL^{-1}	[23]
Glassy carbon electrode + formaldehyde dehydrogenase + poly (glycidyl methacrylate-*co*-3-methylthienyl methacrylate)	Enzymatic	Amperometry	99 μ gL^{-1} – 3 mg L^{-1}	4.5 μ gL^{-1}	[24]
Platinum electrode + chitosan + CdS nanoparticles	Non-enzymatic	Cyclic Voltammetry (CV)	5–50 mg L^{-1} with comparator effect having threshold concentration of 14.85 mg L^{-1}	5 mg L^{-1}	Present work

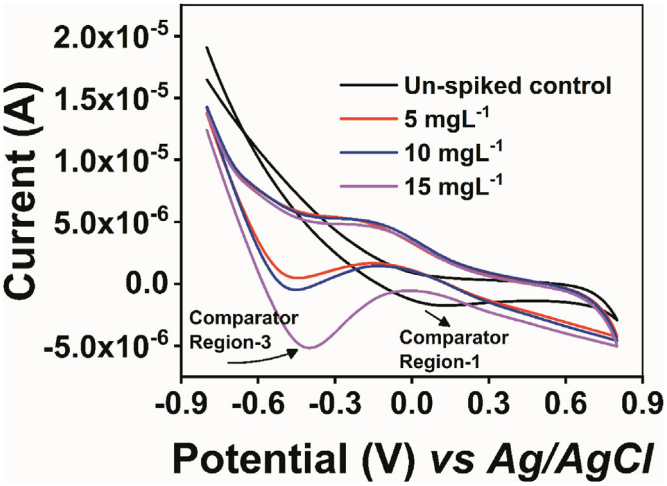

Fig. 7. CV graphs of Pt/Chitosan/CdS modified electrode in 1 mM NaCl in the presence of 5–20 mgL^{-1} of formalin spiked in a fish sample exhibiting the electrochemical comparator effect.

4. Conclusion

A non-enzymatic electrochemical formalin biosensor was designed and developed using CdS nanoparticles as nanointerface employing 1 mM of NaCl as an electrolyte solution. An interesting electrochemical comparator effect was observed during the formalin sensing. Comparator effect was realized in three different cases namely, concentration of formalin < NaCl; concentration of formalin ~ NaCl; and concentration of formalin > NaCl. Their corresponding significance were also investigated and substantiated using the measured electrochemical parameters & calibration curve trends. The threshold concentration of formalin essential for the comparator effect was observed to be 14.845 mgL^{-1}. The sensor exhibited a lower detection limit of 5 mgL^{-1} which is lesser than the allowed usage levels of formalin, it can be used for the precise quantification of formalin levels. The utility of the developed biosensor was vindicated with its versatility in estimating formalin levels in real-time fish samples, with the novel comparator effect.

CRediT authorship contribution statement

Priyannth Ramasami Sundhar Baabu: Formal analysis, Experimental design, conduct of experiments and analysis. **Parthasarathy Srinivasan:** Formal analysis, Conduct of experiments and analysis of results. **Arockia Jayalatha Kulandaisamy:** Formal analysis, Results interpretation and analysis. **Jeyashakila Robinson:** Experimental design, sample selection and real-time studies. **Jeyasekaran Geevaretnam:** Experimental design, sample selection and real-time studies. **John Bosco Balaguru Rayappan:** Conceptualization, Formal analysis, hypothesis design and analysis.

Declaration of competing interest

The authors declare that they have no known competing financial interests or personal relationships that could have appeared to influence the work reported in this paper.

Acknowledgements

We wish to express our sincere thanks to the Department of Science & Technology, New Delhi, India, (SR/FST/ET-II/2018/221) (SERB-EMR/2016/001789) for the financial support. We acknowledge SASTRA Deemed University, Thanjavur, for extending infrastructure support to carry out this work.

Appendix A. Supplementary data

Supplementary data to this article can be found online at https://doi.org/10.1016/j.aca.2020.09.035.

References

[1] FAO, Report of the joint FAO/WHO expert consultation on the risks and benefits of fish consumption. http://www.fao.org/docrep/014/ba0136e/ba0136e00.pdf, January 2010, 2011.
[2] R. Francis-Floyd, Use of formalin to control fish parasites, Coll. Vet. Med. Institue Food Agric. Sci. 77 (1996) 7–9.
[3] IARC, Rep. IARC Working Groups (2004) 401–436, 2006.
[4] S. El Sayed, L. Pascual, M. Licchelli, R. Martínez-Máñez, S. Gil, A.M. Costero, F. Sancenón, Chromogenic detection of aqueous formaldehyde using functionalized silica nanoparticles, ACS Appl. Mater. Interfaces 8 (2016) 14318–14322.
[5] W. Huang, X. Wang, Y. Jia, X. Li, Z. Zhu, Y. Li, Y. Si, B. Ding, X. Wang, J. Yu, Highly sensitive formaldehyde sensors based on polyvinylamine modified polyacrylonitrile nanofibers, RSC Adv. 3 (2013) 22994–23000.
[6] C. Martínez-Aquino, A.M. Costero, S. Gil, P. Gaviña, A new environmentally-friendly colorimetric probe for formaldehyde gas detection under real conditions, Molecules 23 (2018) 2646.
[7] M. Yang, J. He, Graphene oxide as quartz crystal microbalance sensing layers for detection of formaldehyde, Sensor. Actuator. B Chem. 228 (2016) 486–490.
[8] E. Kröber, H. Schäfer, Identification of proteins and genes expressed by methylophaga thiooxydans during growth on dimethylsulfide and their presence in other members of the genus, Front. Microbiol. 10 (2019) 1–14.
[9] B.N. Aini, S. Siddiquee, K. Ampon, Development of formaldehyde biosensor for determination of formalin in fish samples; malabar red snapper (lutjanus malabaricus) and longtail tuna (Thunnus tonggol), Biosensors 6 (2016) 1–15.
[10] N.I. Marzuki, F.A. Bakar, A.B. Salleh, L.Y. Heng, N.A. Yusof, S. Siddiquee, Development of electrochemical biosensor for formaldehyde determination based on immobilized enzyme, Int. J. Electrochem. Sci. 7 (2012) 6070–6081.
[11] T. Shimomura, T. Itoh, T. Sumiya, F. Mizukami, M. Ono, Electrochemical biosensor for the detection of formaldehyde based on enzyme immobilization in mesoporous silica materials, Sensor. Actuator. B Chem. 135 (2008) 268–275.
[12] S.V. Dzyadevych, V.N. Arkhypova, Y.I. Korpan, A.V. El'skaya, A.P. Soldatkin, N. Jaffrezic-Renault, C. Martelet, Conductometric formaldehyde sensitive biosensor with specifically adapted analytical characteristics, Anal. Chim. Acta 445 (2001) 47–55.
[13] S. Ishihara, J. Labuta, T. Nakanishi, T. Tanaka, H. Kataura, Amperometric detection of sub-ppm formaldehyde using single-walled carbon nanotubes and hydroxylamines: a referenced chemiresistive system, ACS Sens. 2 (2017) 1405–1409.
[14] H. Dai, L. Gong, G. Xu, X. Li, S. Zhang, Y. Lin, B. Zeng, C. Yang, G. Chen, An electrochemical impedimetric sensor based on biomimetic electrospun nanofibers for formaldehyde, Analyst 140 (2015) 582–589.
[15] M.R. Baez-Gaxiola, C. Fernández-Sánchez, E. Mendoza, Gold cluster based electrocatalytic sensors for the detection of formaldehyde, Anal. Methods. 7 (2015) 538–542.
[16] Z.L. Zhou, T.F. Kang, Y. Zhang, S.Y. Cheng, Electrochemical sensor for formaldehyde based on Pt-Pd nanoparticles and a Nafion-modified glassy carbon electrode, Microchim. Acta. 164 (2009) 133–138.
[17] Z. Yue, F. Lisdat, W.J. Parak, S.G. Hickey, L. Tu, N. Sabir, D. Dorfs, N.C. Bigall, Quantum-dot-based photoelectrochemical sensors for chemical and biological detection, ACS Appl. Mater. Interfaces 5 (2013) 2800–2814.
[18] P.P. Chandra, A. Mukherjee, P. Mitra, Synthesis of Nanocrystalline CdS by SILAR and Their Characterization, vol. 2014, 2014, p. 138163.
[19] Y.-J. Zhu, F. Chen, Microwave-assisted preparation of inorganic nanostructures in liquid phase, Chem. Rev. 114 (2014) 6462–6555.
[20] M. Mariappan, G. Madhurambal, B. Ravindran, S.C. Mojumdar, Thermal, FTIR and microhardness studies of bisthiourea-urea single crystal, J. Therm. Anal. Calorim. 104 (2011) 915–921.
[21] K. Sing, The use of nitrogen adsorption for the characterisation of porous materials, Colloids Surfaces A Physicochem. Eng. Asp. 187–188 (2001) 3–9.
[22] J. Qian, S. Yan, Z. Xiao, Electrochemical biosensor based on CdS nanostructure surfaces, J. Colloid Interface Sci. 366 (2012) 130–134.
[23] C.R.A.J. Bard, L.R. Faulkner, E. Swain, Electrochemical Methods: Fundamentals and Applications, second ed., Wiley-Blackwell, 2000.
[24] Y. Herschkovitz, I. Eshkenazi, C.E. Campbell, J. Rishpon, Electrochemical biosensor for formaldehyde, J. Electroanal. Chem. 491 (2000) 182–187.
[25] S.K. Ozoner, E. Erhan, F. Yilmaz, P. Ergenekon, I. Anil, Electrochemical biosensor for detection of formaldehyde in rain water, J. Chem. Technol. Biotechnol. 88 (2013) 727–732.